

Stored light and EIT at high optical depths

M. Klein^{a,b}, Y. Xiao^a, M. Hohensee^{a,b}, D. F. Phillips^a, and R. L. Walsworth^{a,b}

^aHarvard-Smithsonian Center for Astrophysics, Cambridge, MA, 02138 USA

^bDepartment of Physics, Harvard University, Cambridge, MA, 02138 USA

August 26, 2021

ABSTRACT

We report a preliminary experimental study of EIT and stored light in the high optical depth regime. In particular, we characterize two ways to mitigate radiation trapping, a decoherence mechanism at high atomic density: nitrogen as buffer gas, and a long, narrow cell geometry. Initial results show the promise of both approaches in minimizing radiation trapping, but also reveal problems such as optical pumping into trapped end-states. We also observe distortion in EIT lineshapes at high optical depth, a result of interference from four-wave mixing. Experimental results are in good qualitative agreement with theoretical predictions.

Keywords: Electromagnetically-induced transparency, slow light, stored light, vapor cell, buffer gas, four-wave mixing, optical depth

1. INTRODUCTION

Using electromagnetically-induced transparency (EIT) techniques to store light for quantum communication applications¹ is a topic of great current interest. Proof-of-principle experiments in both cold and warm atomic systems have successfully demonstrated reversible storage of photon states,²⁻⁴ single-photon EIT,⁵ and the application of stored light techniques in quantum repeaters to increase the efficiency of long distance quantum communication.⁶⁻⁹ Despite this progress, low efficiency of storage and retrieval remains an obstacle on the way to successful long distance quantum communication applications.⁹ Here, we investigate techniques towards improved efficiency in the classical regime for atomic vapor cell systems.

The complete and reversible transfer between photon states and atomic ensemble spin states relies on strong light-atom coupling. Large coupling requires a correspondingly large optical depth. Theory based three-level atom models reveal that stored-light efficiency tends towards 100% provided that the ground state decay rate is zero.¹⁰ In realistic atomic systems, decoherence arises from mechanisms such as collisions with buffer gas atoms and cell walls, diffusion out of the laser beam, and residual magnetic field gradients. When non-zero coherence decay is taken into account, the storage efficiency initially improves with increasing optical depth, but then falls off due to the increasing dominance of absorption associated with the coherence decay. Such a trend has been observed experimentally,^{11,12} but the efficiency peaks at a much smaller optical depth than predicted, indicating that additional loss mechanisms at large optical depth are missing from the straightforward model.

Additional decoherence mechanisms include spin exchange, radiation trapping and unwanted four-wave mixing. The presence of radiation trapping at large optical depth in atomic vapor has been well established.^{11,13} Here, we present progress in our investigations of the effects of radiation trapping on slow and stored light. We report preliminary results on two potential methods to mitigate radiation trapping, namely, by using a nitrogen buffer gas and by using a narrow cell. We also present preliminary results on four-wave mixing effects on EIT. Both the static EIT spectra and the stored light efficiency are measured as diagnostic tools.

2. EXPERIMENTAL SETUP

We used the D_1 transition in a warm ^{87}Rb vapor cell to perform EIT and stored light experiments. The full energy level structure and coupling fields are shown in Fig. 1: a strong control field is resonant with the $F = 2 \rightarrow F' = 2$ transition and a weak probe field with $F = 1 \rightarrow F' = 2$. The atomic medium was in a low magnetic field environment allowing $m = -1$, $m = 0$, and $m = +1$ Zeeman levels to participate in EIT processes (Fig. 1).

arXiv:0812.4939v1 [quant-ph] 29 Dec 2008

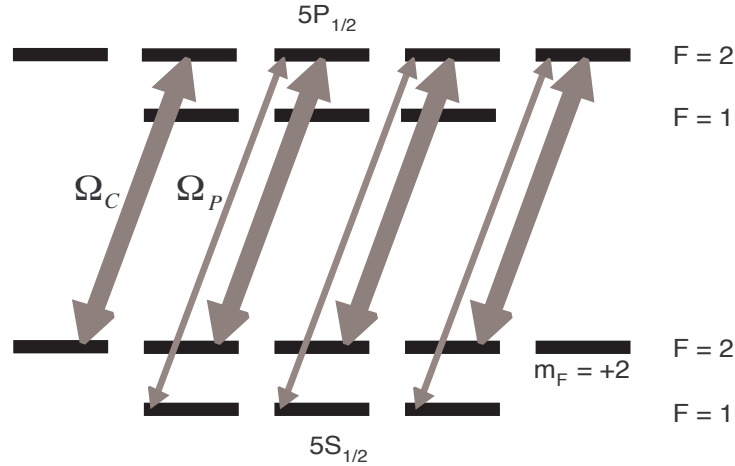


Figure 1. The D₁ structure of ⁸⁷Rb atomic energy levels and coupling fields used in a hyperfine Λ -scheme for EIT and slow and stored light. Both light fields are σ^+ -polarized, with the strong control and weak probe fields denoted by their respective Rabi frequencies Ω_C and Ω_P . The $|F, m_F\rangle = |2, 2\rangle$ Zeeman sublevel acts as a trapped state, where atoms optically pumped into the state cease participating in the EIT process.

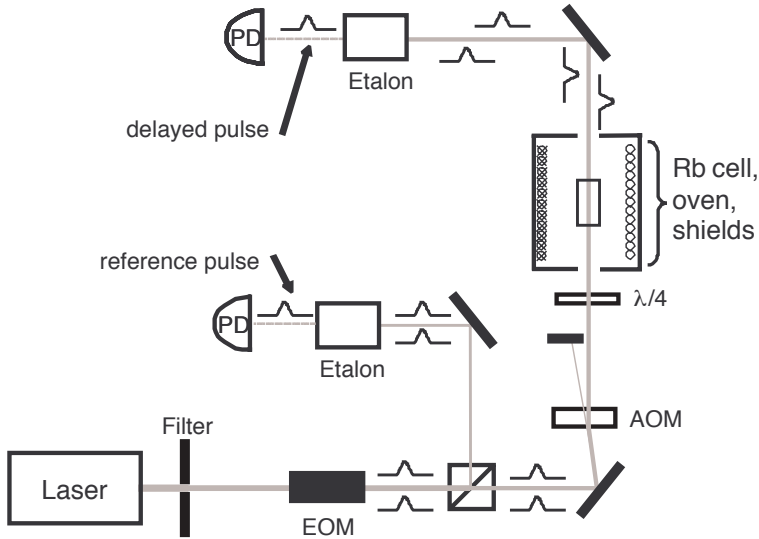


Figure 2. Apparatus used for EIT and stored light measurements in Rb vapor cells. Electro-optic (EOM) and acousto-optic (AOM) modulators temporally shape the probe and control fields which enter a rubidium (Rb) vapor cell housed inside an oven with solenoid, and magnetic shielding. Etalons are used to pass only the probe light onto photodetectors (PD). *See text for details.*

The optical fields were generated by an external cavity diode laser tuned to $\lambda = 795$ nm, amplified by a tapered amplifier, and spatially filtered through a pinhole as shown in Fig. 2. The amplified laser power after the pinhole was 70 mW. A 6.8 GHz resonant electro-optic modulator (EOM), driven with ~ 1 W of rf power, phase modulated the laser light at the ground state hyperfine splitting (~ 6.835 GHz); the carrier acted as the control field, and the +1 sideband as the probe field, with a maximum probe to control intensity ratio of 4%. The sideband amplitude was varied to shape the desired probe pulse for stored light measurements. The EOM drive frequency was varied to change the two-photon detuning δ of the EIT transition for measuring its lineshape. For stored light measurements, both the drive and the probe fields were quickly turned off by the AOM while the slow pulse traveled through the vapor cell, storing the pulse in the medium. Then the control field was turned on after a storage interval.

After an acousto-optic modulator (AOM) set the intensity of the light, a quarter-wave plate ($\lambda/4$) converted it from linear to circular polarization. The collimated beam entering the cell had a diameter of approximately 6.8 mm. At the Rb cell output, a temperature-stabilized etalon (free spectral range 20 GHz and extinction ratio of ~ 200) was used to filter the control field light and transmit only the probe light onto a photodetector (PD). An etalon was used to attain the high bandwidth needed for detection of short pulses. The transmission of the -1 EOM sideband (with δ set off resonance), was used as a reference for determining the off resonant transmission level of the probe. With the carrier detuned ~ 13 GHz below the probe transition frequency $1 \rightarrow 2$, the -1 sideband is 20 GHz detuned, and thus transmitted by the next etalon resonance. A small amount of input light was picked off earlier in the beam path and sent to a separate temperature-stabilized etalon, and this signal was used as a reference for slow light time delay measurements; slow light delay was defined as the difference in peak arrival times between the reference and output probe pulses.

The Rb vapor cell was housed inside a plastic oven, which was heated by blown warm air. The cell temperature was varied between 39 and 79 °C, or atomic number density between 3.8×10^{10} and 1.1×10^{12} cm $^{-3}$. Three layers of cylindrical high-permeability shielding surrounded the oven to screen out stray laboratory magnetic fields, and a solenoid inside was used to cancel any small constant background field. Three Rb vapor cells were used in our experiments; all three contained isotopically enriched ^{87}Rb and were filled with buffer gas to confine atoms and extend their coherence life times. Two cells had length $L = 15$ cm and diameter $D = 1.2$ cm, one filled with 40 torr of Ne buffer gas and the other with 25 torr of N $_2$. The third also contained 40 torr of Ne, and had dimensions $L = 7.5$ cm and $D = 2.5$ cm. The unusually long aspect ratio was used to combat the effects of radiation trapping, as described below. These cell choices allowed us to directly investigate the role of different buffer gases (by comparing the two long cells), and the role of cell geometry (by comparing the two Ne buffer gas cells).

3. COMPARISON OF NEON AND NITROGEN BUFFER GAS VAPOR CELLS

We compared the use of Ne and N $_2$ buffer gases in EIT with the aim of mitigating radiation trapping in stored light media. Radiation trapping occurs when atoms absorb input light, then undergo spontaneous emission; these emitted photons can then be re-absorbed and re-emitted multiple times before escaping an optically-thick atomic medium. Since spontaneously-emitted photons have random polarization, re-absorbed photons act to equilibrate the population distribution among different Zeeman sublevels, reducing the optical pumping efficiency and coherence lifetime. Radiation trapping can significantly impact the polarization of an EIT medium^{11, 13} and thus potentially the efficiency of stored light.

To reduce the negative effects of radiation trapping, we tested nitrogen as buffer gas, as nitrogen de-excites the Rb atoms without scattering photons by transferring the energy to vibrational states in the N $_2$ molecules.¹³ We note that many optical pumping experiments have used nitrogen for this purpose but these studies use much higher nitrogen pressure than we report here in EIT experiments.¹⁴ We used two identical ^{87}Rb vapor cells, one with 40 torr of Ne, and the other with 25 torr of N $_2$ chosen such that the excited state pressure broadening (γ) was the same in both cells. The nominal optical pumping rate, Ω_C^2/γ , was then the same in both cells for a given laser power. Since radiation trapping depolarizes and decoheres the atomic ground state, we used measurements of EIT (which is based on ground state coherence) in the two cells to study the effect of radiation trapping.

EIT is sensitive to both optical depth and ground state decoherence, and is thus a useful proxy for stored light experiments.¹⁵ In particular, the off-resonant floor of an EIT spectrum is determined by the effective optical

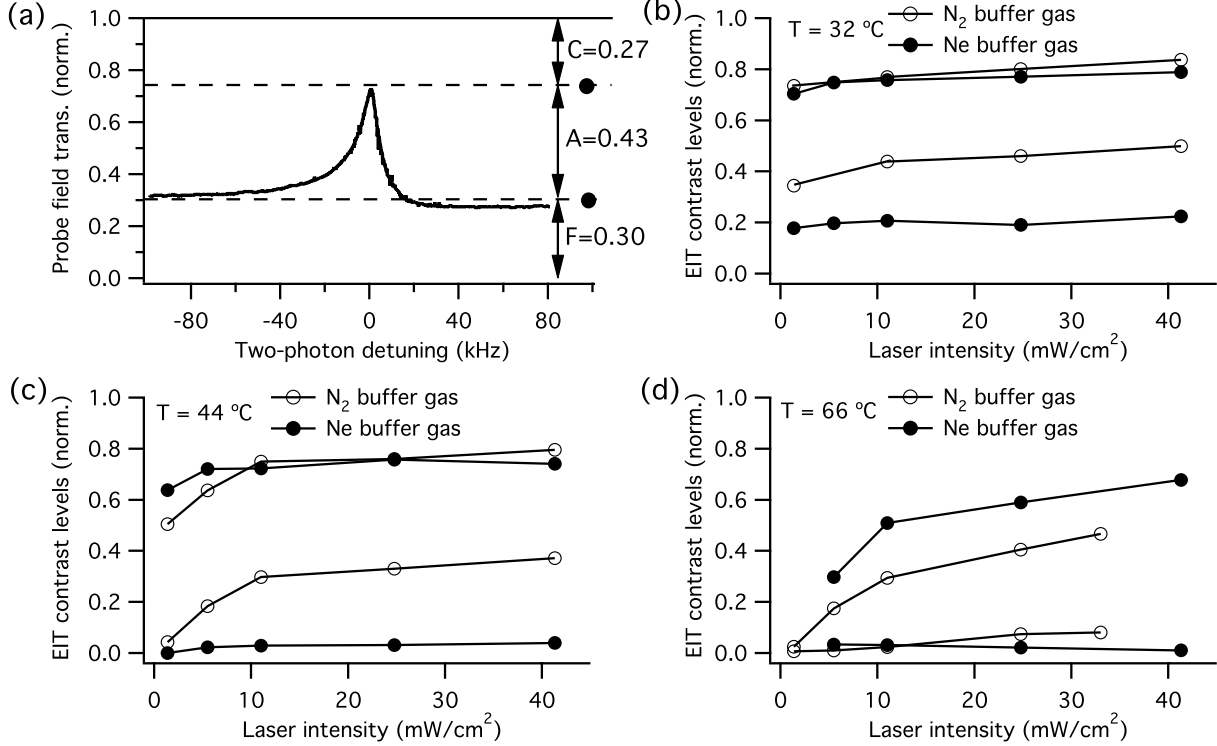


Figure 3. Neon and nitrogen buffer gas comparison, demonstrating reduced effective optical depth in N_2 . (a) Typical EIT spectrum, normalized to the full off-resonant probe transmission level. The contrast levels are labeled by F , the off-resonant transmission level, which is a measure of the system’s optical depth; A , the EIT amplitude; and C , the normalized difference between full transmission (away from the Rb D_1 transition) and the peak of the EIT spectrum. EIT resonance measured at $T = 44$ °C and laser power 4 mW. EIT contrast levels F and $F + A$ vs. laser intensity for both Ne and N_2 are shown for Rb cell temperatures (b) $T = 32$ °C, (c) $T = 44$ °C, and (d) $T = 66$ °C.

depth d : $F = \exp(-d)$, where d is proportional to the optical path length, the atomic density, and the fraction of atoms in the relevant atomic levels. The peak transmission is determined by the control field Rabi frequency, the effective optical depth d and the ground state coherence decay rate γ_0 : $F + A = \exp(-d\gamma_0/\Omega_C^2)$. Here, the floor (F) and amplitude (A) are normalized to the off-resonant transmission level of the probe light, as shown in Fig. 3(a). In general, a lower floor and a higher EIT transmission are desirable for stored light experiments.

We observed lower EIT floors and higher peak transmissions in neon buffer gas cells than N_2 cells (Fig. 3). Therefore, we expect reduced stored-light performance from the N_2 buffer gas cell in comparison to the neon cell. We believe the increased EIT floor in the N_2 cell was predominantly due to increased population in the $|F = 2, m_F = 2\rangle$ end state. The σ^+ polarization of the control and probe light led to optical pumping into this state, which was then inaccessible to the EIT process, effectively reducing the optical depth and raising the EIT floor. As seen in Fig. 3, the floor level increased with laser intensity in both cells because more atoms were pumped to the end state at high laser intensity. The higher EIT floor in the N_2 buffer gas cell was indicative of more efficient optical pumping to the trapped state, and poorer performance for slow and stored light.

Since radiation trapping reduces optical pumping efficiency, the higher trapped state population in the N_2 cell may indicate that this cell had less radiation trapping. However, the population distribution as Rb de-excites to the ground state in the presence of different buffer gases may also play a role. We carried out a full 16-level density matrix simulation of both cells in the optically thin regime, and found that if the Rb atoms are quenched to the ground state with the same m_F state before excited state mixing occurs (as in the N_2 cell) there is a higher population in the trapped state. However, if Rb is allowed to de-excite to all allowed ground states (as in the Ne cell, since the excited states are uniformly mixed before spontaneous emission), then there is less population

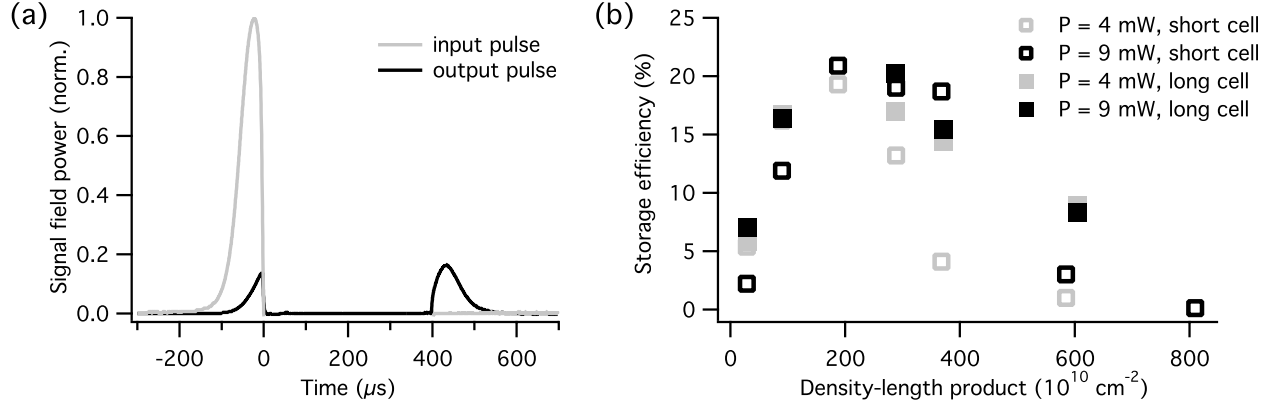


Figure 4. Stored light in Ne buffer gas cells, and the dependence on geometry. (a) Example stored light measurement in the long, narrow 40 torr Ne buffer gas cell. The input reference pulse is normalized to the off-resonant transmission level for the probe field. The output probe pulse consists of a leaked part, escaping before the control field is shut off, then a readout after a 400 μ s storage interval. Leakage is present because the entire pulse is not spatially compressed enough to fit inside the cell. $T = 57$ °C, and the laser beam diameter and power $d = 6.8$ mm and $P = 9$ mW. Efficiency is defined as the area of the output pulse divided by the area of the input pulse, here 20.3%. (b) Geometry-dependence of stored light, using Ne buffer gas cells. At high optical depth, the short cell yields very low efficiency, while the long, narrow cell has significantly greater efficiency. We attribute the improved storage efficiency to a reduction in radiation trapping due to reduced transverse optical depth from both a smaller cell diameter and lower Rb density.

in the trapped state. Detailed modelling of the population distribution after optical pumping requires branching ratios of Rb de-excitation in the presence of various buffer gases and further study will be required.

The N₂ buffer gas cell also showed lower peak EIT transmission (Fig. 3) due to the larger ground state decoherence rate in the nitrogen cell. We also measured the ground state coherence decay rate by the 1/e time of stored light efficiency vs. storage time, and found a decoherence rate that was four times greater in the nitrogen cell. Shorter atom-light interaction time (the diffusion time) in the nitrogen cell contributed to this increase in decoherence. The N₂ buffer gas did not provide better EIT than Ne buffer gas, due to increased pumping of Rb atoms into the trap state. While further work is needed to understand the details of Rb de-excitation, other techniques must also be developed to reduce the effects of radiation trapping in stored light vapor cells.

4. NARROW VAPOR CELL GEOMETRY

In addition to using nitrogen buffer gas to quench the excited state in Rb atoms, radiation trapping can be mitigated by using a long, narrow cell geometry. A narrow cell allows fluorescence to escape the cell in the transverse direction with fewer depolarizing interactions with Rb atoms. When the transverse diameter of the cell is kept below one optical depth of the Rb medium, most radiated photons escape before undergoing additional interactions with the Rb vapor. (Such aspect ratios were also investigated in a cold atom cloud, where radiation trapping was reduced, enabling laser cooling to much higher phase-space densities.¹⁶) A longer cell can reach the same optical depth with a lower atomic density, allowing the vapor cell to be heated to lower temperatures and reducing additional density-dependent effects such as spin-exchange collisions.

To test the effects of cell aspect ratio, we compared stored light results in two 40 torr Ne buffer gas cells with different geometries: a longer cell with $D = 1.2$ cm and $L = 15$ cm, and a shorter cell with $D = 2.5$ cm and $L = 7.5$ cm. Optimal stored-light efficiency was measured using an iterative optimization process^{17,18} as a function of optical depth for a fixed storage time of $\tau = 400$ μ s, at two laser powers. Initial results (Fig. 4) showed improved efficiency in the long cell than the short cell. At high optical depth, the long cell yielded much higher efficiency, indicative of reduced radiation trapping in the high aspect ratio cell. However, the theoretically expected larger overall efficiency¹⁰ was not achieved. We attribute this to the presence of greater magnetic field inhomogeneity in the long cell. The addition of higher order compensating coils will reduce this inhomogeneity

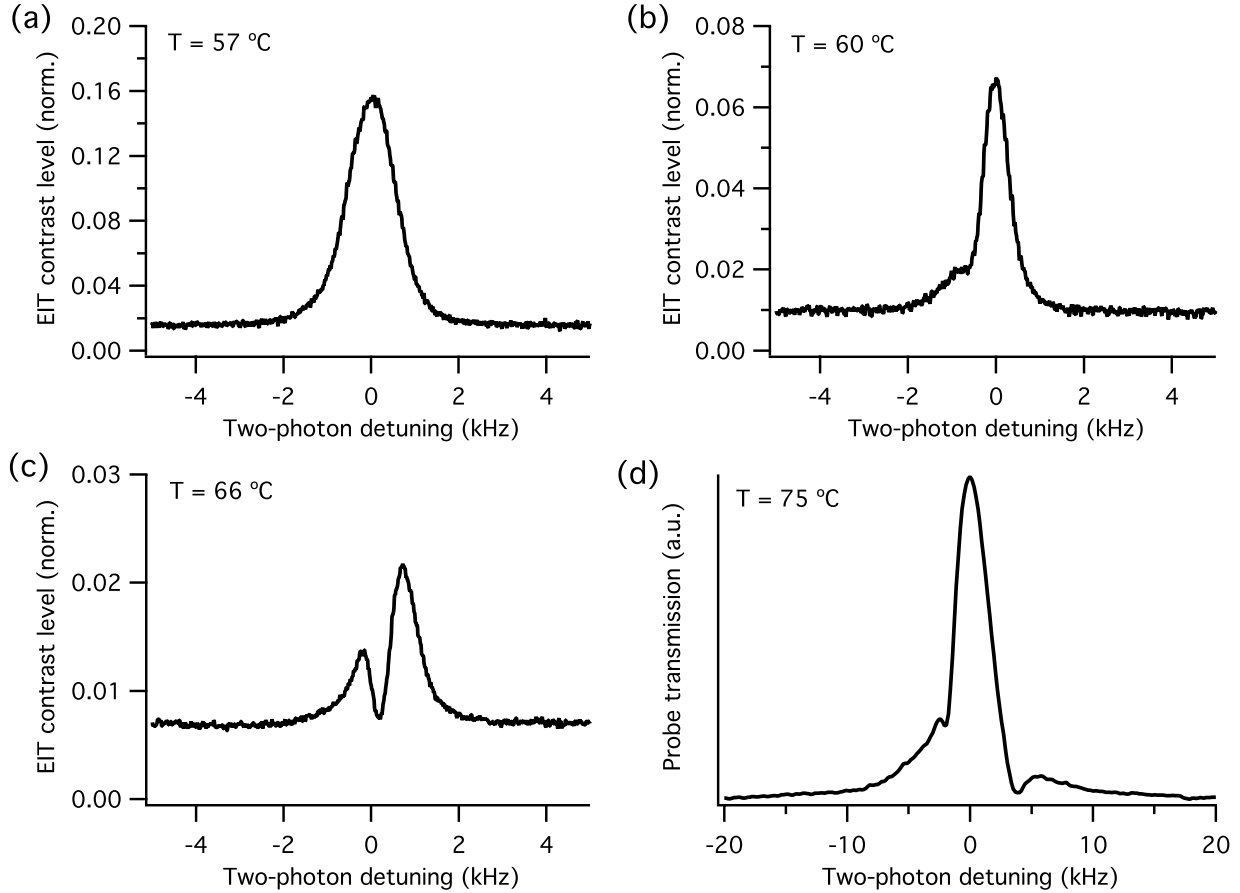


Figure 5. Additional peaks in EIT spectra due to four-wave mixing. (a-c) Using the long, narrow N_2 buffer gas cell, for a fixed input power of $P = 500 \mu\text{W}$ at respective temperatures of $T = 57 \text{ }^\circ\text{C}$, $T = 60 \text{ }^\circ\text{C}$, and $T = 66 \text{ }^\circ\text{C}$. (d) Using the 7.5 cm Ne buffer gas cell at $T = 75 \text{ }^\circ\text{C}$, with input power $P = 8.8 \text{ mW}$, we observe three peaks in the spectrum; relative size of the four-wave mixing peaks is diminished at this much higher laser intensity.

and may improve the storage efficiency. Our measurements suggest that a high aspect-ratio cell is a route towards improved efficiency.

5. EFFECTS OF FOUR-WAVE MIXING

Although electromagnetically induced transparency describes most of the physics in the Rb medium coupled to two optical input fields, four-wave mixing plays an important role in the high-density limit because its efficiency scales with the square of the density. The control field can interact with the probe transition, generating an anti-stokes field, and forming a four-wave-mixing cycle. Although the drive field is detuned from the probe's resonance by 6.8 GHz, EIT ground state coherence can enhance the efficiency of nonlinear wave mixing.¹⁹ Furthermore, in our experiment, the unwanted -1 sideband of the EOM coincides with the (control-probe-control)-generated anti-stokes resonance and seeds four-wave mixing. Four-wave mixing coexisting with EIT has been reported in several experiments.^{12, 20, 21} For example, EIT with multiple peaks (oscillations or fringes) caused by four-wave mixing was observed in a high optical depth Rb sample cooled by buffer gas.²¹ Wave mixing can also cause gain in the weak probe. We have directly observed greater than 100% transmission of the probe light in a miniature paraffin-coated cell.²² This gain induces noise which can destroy quantum correlations in the photon pairs generated in such systems.²³

We studied EIT lineshapes for several different optical depths (Fig. 5). Since EIT lineshapes can be changed by adjusting the one-photon detuning,²⁴ we set the laser to resonance with $F = 2$ excited state to simplify analysis. However, the EIT contrast improved when the laser was detuned from the $F = 2$ resonance; in particular, the stored light efficiency was higher when the laser was tuned to the $F = 1$ excited states than to the $F = 2$, which we attribute to an effectively lower optical depth from the reduced coupling of the transition to the $F = 1$ transition. At large optical depths the EIT lineshape had multiple peaks or fringes^{20,21} as shown in Fig. 5, and consistent with theoretical analysis.^{20,21} Fringes in the EIT resonance reduce the useful transparency window and the stored light efficiency. The period of the fringes in an EIT lineshape contaminated by four-wave mixing is $\sim \Omega_C^2/\gamma d$, where d is the homogeneous optical depth, and the EIT linewidth is $\Omega_C^2/\gamma\sqrt{d}$.²⁰ The fringe period scales linearly with d^{-1} , reflecting the dispersive characteristics of the system and the number of oscillations in the EIT resonance scales as \sqrt{d} . At high optical depth the efficiency of four-wave mixing is also higher, increasing the fringe contrast. Therefore the contrast and number of fringes in the EIT spectrum can be used as a diagnostic of the optical depth and four-wave mixing in the system and set an upper limit on the available optical depth for good stored light performance in a vapor cell. Further study is needed to evaluate the negative effect of four-wave mixing on stored light efficiency (though the efficiency of the retrieved anti-stokes field has been studied previously¹²). Active elimination of four-wave mixing via sophisticated polarization schemes have also been proposed theoretically.²⁵

6. CONCLUSIONS

We have reported a preliminary experimental study of EIT and stored light aimed at understanding performance at high optical depth. We compared N₂ and Ne buffer gases, and studied stored light efficiency in long, narrow vapor cells. Initial results with both N₂ and long, narrow cells show promise for reducing the effects of radiation trapping. Pumping of population into trapped end states needs to be addressed before one can make effective use of an N₂ buffer gas cell. The long, narrow cell is also a promising route to high efficiency with improved magnetic field compensation. We also observed multiple peaks in EIT lineshapes, which became stronger at high optical depth due to interference between EIT and a four-wave mixing channels. Experimental results were in good qualitative agreement with theoretical predictions.

We are grateful to I. Novikova for useful discussions. This work was supported by ONR, DARPA, NSF, and the Smithsonian Institution.

REFERENCES

1. M. D. Lukin, Rev. Mod. Phys. **75**, 457 (2003).
2. C. H. Van der Wal, M. D. Eisaman, A. Andre, R. L. Walsworth, D. F. Phillips, A. S. Zibrov, M. D. Lukin, Science **301**, 196 (2003).
3. K. S. Choi, H. Deng, J. Laurat et.al., Nature **452**, 67 (2008).
4. T. Chaneliere, D. N. Matsukevich, S. D. Jenkins, et al., Nature **438**, 833 (2005).
5. M. D. Eisaman, A. André, F. Massou, M. Fleischhauer, A. S. Zibrov, and M. D. Lukin, Nature **438**, 837 (2005).
6. L. M. Duan, M. D. Lukin, J. I. Cirac, and P. Zoller, Nature **414**, 413 (2001).
7. C. W. Chou, J. Laurat, H. Deng, et al., Science **316**, 1316 (2007).
8. D. N. Matsukevich, T. Chaneliere, S. D. Jenkins, et al., Phys. Rev. Lett. **96**, 030405 (2006).
9. Z. S. Yuan, Y. A. Chen, B. Zhao, et al., Nature **454**, 1098 (2008).
10. A. V. Gorshkov, A. Andre, M. D. Lukin, and A. S. Sorensen, Phys. Rev. A **76**, 033805 (2007).
11. M. Klein, Y. Xiao, A. V. Gorshkov, M. Hohensee, C. D. Leung, M. R. Browning, D. F. Phillips, I. Novikova and R. L. Walsworth, Proc. SPIE-Int. Soc. Opt. Eng. **6904**, 69040C-1 (2008).
12. N. B. Phillips, A. V. Gorshkov, and I. Novikova, Phys. Rev. A **78**, 023801 (2008).
13. A. F. Molisch and B. P. Oehry, *Radiation Trapping in Atomic Vapors* (Oxford University Press, USA, 1999); A. B. Matsko, I. Novikova, M. O. Scully, and G. R. Welch, Phys. Rev. Lett. **87**, 133601 (2001); A. B. Matsko, I. Novikova, and G. R. Welch, J. Mod. Opt. **49**, 367 (2002).

14. M. A. Rosenberry, J. P. Reyes, D. Tupa, and T. J. Gay, Phys. Rev. A **75**, 023401(2007); M. Schiffer, E. Cruse and W. Lange, Phys. Rev. A **49**, R3178 (1994).
15. M. Klein, M. Hohensee, Y. Xiao, R. Kalra, D. F. Phillips, R. L. Walsworth, to be published.
16. M. Vengalattore, R. S. Conroy, M. G. Prentiss, Phys. Rev. Lett. **92**, 183001 (2004).
17. A. V. Gorshkov, A. Andre, M Fleischhauer, A. S. Sorensen, and M. D. Lukin, Phys. Rev. Lett. **98**, 123601 (2007).
18. I. Novikova, A. V. Gorshkov, D. F. Phillips, A. S. Sorensen, M. D. Lukin, and R. L. Walsworth Phys. Rev. Lett. **98**, 243602 (2007); I. Novikova, A. V. Gorshkov, D. F. Phillips, Y. Xiao, M. Klein, and R. L. Walsworth, Proc. SPIE-Int. Soc. Opt. Eng. **6482**, 64820M-1 (2007).
19. M. Jain, H. Xia, G. Y. Yin, A. J. Merriam, S. E. Harris, Phys. Rev. Lett. **77**, 4326 (1996).
20. M. D. Lukin, M. Fleischhauer, A. S. Zibrov, H. G. Robinson, V. L. Velichansky, L. Hollberg, and M. O. Scully Phys. Rev. Lett. **79**, 2959 (1997).
21. T. Hong, A. V. Gorshkov, D. Patterson, A. S. Zibrov, J. M. Doyle, M. D. Lukin, and M. G. Prentiss, e-print archive quant-ph/0805.1416v1 (2008).
22. M. Klein, M. Hohensee, Y. Xiao, D. F. Phillips, R. L. Walsworth, to be published.
23. S. Manz, T. Fernholz, J. Schmiedmayer, and J. Pan, Phys. Rev. A **75**, R040101 (2007).
24. E. E. Mikhailov, V. A. Sautenkov, I. Novikova, et al., Phys. Rev. A. **69**, 063808 (2004).
25. M. Hohensee et al., to be published.